Appl. Phys. B 67, 769–772 (1998)

Applied Physics B
Lasers
and Optics

Rapid communication

Gaussian-like tapered grating quarter wave-shifted DFB semiconductor lasers for high-power single-mode operation

T. Fessant

c/o Hélène Conan, 6 rue F. Le Guyader, 29200 Brest, France

Received: 27 July 1998/Revised version: 25 September 1998

Abstract. Theoretical threshold and above-threshold investigations on quarter wave-shifted distributed feedback (QWS-DFB) lasers with a gaussian-like tapered grating are presented. It is shown that a wide range of longitudinal coupling coefficient variations with gaussian profiles may lead to devices with very large gain margins combined with sufficiently flat intra-cavity fields, so that modal instabilities induced by spatial hole burning can be avoided. Apart from the benefits of keeping a nearly constant side mode suppression ratio above threshold, these specific structures may also exhibit an enlarged output optical power with respect to conventional QWS-DFB lasers, since the spatially dependent coupling coefficient alters the field distribution inside the cavity.

PACS: 42.55.Px; 42.79.Yd; 07.05.Tp

In the past decade, conventional quarter wave-shifted distributed feedback (QWS-DFB) lasers have been studied, extensively reported in the literature, technologically realized and implemented in optical fiber telecommunication systems. Their main advantage is related to the structural characteristics of the Bragg grating: a built-in phase shift which makes them oscillating in a single longitudinal mode at threshold, with a good mode discrimination. However, problems may occur in the above-threshold regime where spatial hole burning (SHB) takes place, degrading the side mode suppression ratio (SMSR), especially for strongly coupled devices (coupling–length product $\kappa L > 1.25$). Although it has been shown that this peculiar value of κL was optimum in terms of single-mode stability [1], higher κL products are desirable because of their lower threshold current, smaller linewidth–power products and lower reflection sensitivity [2], so that further optimization is required.

Various solutions have been proposed to overcome the SMSR degradation in purely index coupled structures, by enlarging the threshold gain margin and/or by flattening the intra-cavity field: longitudinally dependent coupling coefficients in QWS-DFB structures [3–5], multiple discrete phase shifts located along the cavity [6, 7], use of chirped gratings [8–10] or phase-adjustment regions (PAR) [11, 12], as well as an adequate combination of a PAR and a stepwise constant coupling coefficient [13].

Recent works deal with a new concept of biharmonic Bragg resonator, which is a combination of two superimposed sinusoidal gratings of equal height but slightly different period, resulting in a sinusoidal space-modulated coupling coefficient [14, 15]. To some extent, the biharmonic structure may be compared to our specific device and further explanations are given below.

1 Scope of the study

The proposed multisection structure is depicted on the top of Fig. 1. A tapered grating, leading to continuous changes of the coupling coefficient κ along the structure, is combined with a $\lambda/4$ phase shift at the center of the cavity. Since we are here only interested in the theoretical behavior of gaussian-like tapered grating (GLTG) QWS-DFBs, practical problems linked to their technological realization are not addressed. So,

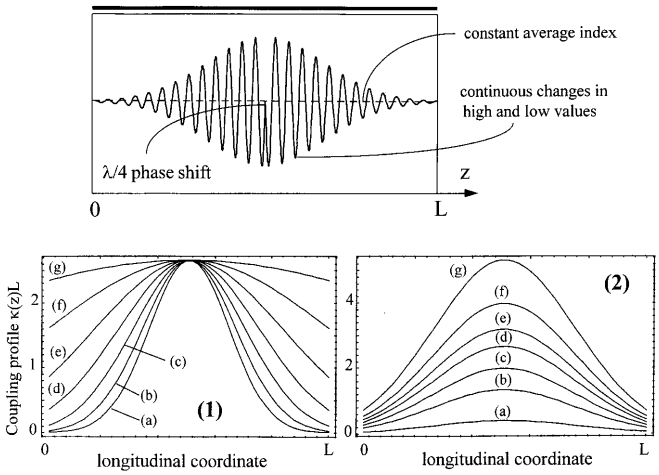

Fig. 1. *Top:* schematic view of a gaussian-like tapered grating (GLTG) QWS-DFB laser. *Bottom* (1) and (2): coupling coefficient profiles used for the numerical simulations and collected in Table 1

a major simplifying hypothesis is that the longitudinal variation of κ does not induce any effective index variation or alternatively, that these index variations can be compensated for by a longitudinally dependent grating pitch. It means that the high and low values of the effective index are changed independently of its average value. κ is assumed to follow a gaussian spatial dependence and can thus be expressed as

$$\kappa(z) = \frac{1}{\sqrt{2\pi}\sigma} \exp\left(-\frac{(z - L/2)^2}{2\sigma^2}\right). \quad (1)$$

Let us now discuss some basic structural differences between the GLTG-QWS-DFB and the biharmonic structure proposed in references [14, 15]: The first fundamental difference lies in the Bragg structure geometry itself: two superimposed sinusoidal gratings of equal height but slightly different period in the biharmonic device, compared with a single and amplitude modulated grating, provided with a discontinuity, in the GLTG-QWS-DFB laser. In the biharmonic device, no phase shift is required since the lasing mode is found to oscillate exactly at the Bragg frequency thanks to the asymmetric nature of the sinusoidal coupling coefficient. In contrast, the GLTG-QWS-DFB structure requires a $\lambda/4$ phase shift (a discontinuity of π in the corrugation) to obtain stable single-mode operation.

The second discrepancy lies in the longitudinal profile of the coupling coefficient $\kappa(z)$. It must be noted that, compared to references [14, 15], our definition of $\kappa(z)$ does not include the grating phase which is treated separately. So, with respect to these papers, $\kappa(z)$ in (1) represents the modulus of the coupling strength, which appears to be symmetric with respect to the center of the cavity $L/2$. Now, with the conventions of references [14, 15], an asymmetric and spatially dependent coupling coefficient, with a phase shift at $L/2$, would have been defined. So, in the GLTG-QWS-DFB laser, the modulus of $\kappa(z)$ is maximum at $L/2$ and decreases towards the ends of the cavity while its phase exhibits a discontinuity at $L/2$; in the biharmonic structure, $\kappa(z)$ is continuous everywhere, minimum at $L/2$ and its modulus increases towards the ends of the device.

The studied coupling profiles are shown on the bottom of Fig. 1. First, the height of the gaussian function is kept constant but its width is varied ((1-a)→(1-g)). Second, the ratio between the maximum and minimum values of κ, respectively $\kappa_{\max}$ and $\kappa_{\min}$, is unchanged but the gaussian curve is shifted up ((2-a)→(2-g)).

2 Threshold analysis

The threshold analysis is performed by solving the coupled wave equations (CWE) in the frame of a matrix formalism. For the calculations, $\kappa(z)$ is segmented into 50 discrete values, which represents a good compromise between accuracy and computer time consuming. The transfer matrix of the whole structure is thus formed and by applying a numerical procedure based on the secant method in the complex plane, the modes are determined through their locations (δL: detuning with respect to the Bragg wavelength, αL: net gain required to reach threshold). As far as a discrete phase shift equivalent to $\lambda/4$ is located inside the cavity, the lasing mode oscillates exactly at the Bragg wavelength $\delta L = 0$. Like in standard QWS-DFBs, the net gain αL decreases with the increase of the average coupling coefficient $\kappa_{\text{av}}L$ since more feedback is provided in the structure (Table 1).

What is really essential in designing single-mode sources is, first, the threshold gain margin $\Delta\alpha L$ and, second, the flatness F of the intra-cavity field defined as the ratio between the maximum and minimum photon density. Let us first consider the set of coupling profiles (1-a) to (1-g). $\Delta\alpha L$ decreases when $\kappa(z)$ flattens, i.e. when the GLTG-QWS-DFB tends towards the conventional QWS-DFB. On the other hand, for the set of coupling profiles (2-a) to (2-g) which exhibits more and more discrepancies between the high and low values of $\kappa(z)$, $\Delta\alpha L$ increases with $\kappa_{\text{av}}L$. Such a phenomenon was predicted in multisection DFBs provided with a step-

Table 1. Summary of threshold properties of several GLTG-QWS-DFBs

Normalized coupling profile $\kappa(z)L$	Average normalized coupling coefficient $\kappa_{\text{av}}L$	Normalized threshold net gain αL		Normalized threshold gain margin $\Delta\alpha L$	Field flatness F at threshold
(1-a)	0.933	3.353	$(1.616)^{\dagger}$	2.788	11.63 (u)
(1-b)	1.086	2.594	$(1.42)^{\dagger}$	2.349	5.495 (u)
(1-c)	1.292	1.918	$(1.202)^{\dagger}$	1.917	2.884 (u)
(1-d)	1.566	1.353	$(0.97)^{\dagger}$	1.527	2.006 (c)
(1-e)	1.904	0.921	$(0.749)^{\dagger}$	1.197	2.747 (o)
(1-f)	2.262	0.632	$(0.572)^{\dagger}$	0.943	4.021 (o)
(1-g)	2.548	0.473	$(0.461)^{\dagger}$	0.781	5.584 (o)
(2-a)	0.235	4.309	$(3.437)^{\dagger}$	0.661	34.53 (u)
(2-b)	0.783	2.449	$(1.846)^{\dagger}$	1.142	4.701 (u)
(2-c)	1.174	1.801	$(1.321)^{\dagger}$	1.360	2.498 (u)
(2-d)	1.566	1.353	$(0.97)^{\dagger}$	1.527	2.006 (c)
(2-e)	1.879	1.083	$(0.764)^{\dagger}$	1.635	2.718 (o)
(2-f)	2.349	0.778	$(0.536)^{\dagger}$	1.766	4.414 (o)
(2-g)	3.312	0.445	$(0.259)^{\dagger}$	1.927	10.145 (o)

(u): undercoupling, (c): critical coupling, (o): overcoupling, $(...)^{\dagger}$: threshold net gain of the standard QWS-DFB with equivalent average coupling coefficient

wise constant coupling coefficient [13]: A stronger coupling at the center of the cavity leads to an enlargement of $\Delta\alpha L$, especially when the lasing mode oscillates near the Bragg frequency. In fact, with respect to a uniform coupling, the light is less confined at the ends of the cavity, the feedback is lower and each mode requires a higher gain to reach threshold. However, this shift is not homogeneous because of a complex mode competition, typical for non-constant-κ devices, which induces a kind of apparent absorption or gain [16]. Indeed, from a mathematical point of view, a spatial modulation of κ has the dimension of absorption, so that an additional term enters the CWE, each mode being affected differently.

Figure 2 displays the performance of various GLTG-QWS-DFB laser diodes in the ($\Delta\alpha L$, F) plane for several coupling values. Obviously, the structural optimization requires an as large as possible $\Delta\alpha L$ combined with an F parameter approaching unity (perfectly flat field). The two GLTG-QWS-DFB curves are significantly shifted towards higher $\Delta\alpha L$ with respect to conventional QWS-DFBs. The value of F is limited by the presence of the phase shift but, in the region marked by a dashed ellipse, F remains relatively moderate and a wide range of GLTG-QWS-DFBs are optimal for single-mode operation. Note also that the intra-cavity fields may be either overcoupled when $\kappa_{\mathrm{av}}L$ is large, or undercoupled in the opposite case. The coupling profile (1-d) is the better compromise between $\Delta\alpha L$ and F, and corresponds to a critical coupling since the field is very flat. It must be emphasized that, compared to biharmonic structures [14, 15], GLTG-QWS-DFB cavities are liable to exhibit significantly larger gain margins but will fail to yield very uniform intracavity fields because of the cusp produced in the internal photon density by the localized phase shift. Indeed, for that latter purpose, the sinusoidal coupling profile of biharmonic devices (weak coupling at the cavity center), associated with an "accumulated" phase shift along the cavity (no need for localized phase shift), leads probably to achieve flatter internal fields. So, both structures exhibit distinct advantages and potential.

As indicated in Table 1, the net threshold gain αL is another important parameter of high-power laser diodes because it conditions the required bias current above threshold. From this particular point of view, GLTG-QWS-DFBs are not advantageous with respect to conventional QWS-DFBs since the losses (and thus αL) become higher. As an example, with typical structural and material parameters [13], the threshold current obtained for case (1-d) is 21.97 mA while for its standard counterpart (same αL), it is only 18.85 mA. However, even if GLTG-QWS-DFBs exhibit higher threshold currents than their conventional counterparts, the benefits of keeping a better single-mode behavior dominate in telecommunications systems, as has been emphasized throughout this paper. So, as far as the spectral stability of the structure (which is what we are interested in) depends on the value of the coupling constant, which itself determines both the field distribution and the gain margin, not αL but really κL (or $\kappa_{\mathrm{av}}L$) constitutes the critical parameter in our analysis.

3 Above-threshold analysis

An above-threshold analysis has been performed in order to evaluate the output characteristics as well as the modal stability (with respect to the onset of a side mode) of the optimized structure (1-d). Typically 500–1000 subsections are used by the simulator which solves the CWE and the carrier rate equation in a self-consistent way. Figure 3 displays the photon density profile of both GLTG and standard QWS-DFBs identically coupled ($\kappa L = 1.566$) for several values of the normalized current density (J_{TH} is the threshold current density). It is clear that, due to the phase shift, the two curves are almost identical at the center of the cavity but depart from each other at its ends as a result of the z-dependent κ. Consequently, the GLTG-QWS structure exhibits a larger output optical power, which obviously constitutes the first advantage of the gaussian-like coupled structure.

As a result of a high $\Delta\alpha L$ and a flat field, structure (1-d) is very stable and the emission spectrum remains single-mode with nearly no distortion, even at high bias current (Fig. 4a). A SMSR of more than 50 dB is maintained over the whole range of bias currents (top curve of Fig. 4d). The shift in the emission wavelength between $J = 1.2J_{\mathrm{TH}}$ and $J = 6J_{\mathrm{TH}}$ is 0.22 nm. It must be mentioned that temperature effects, which

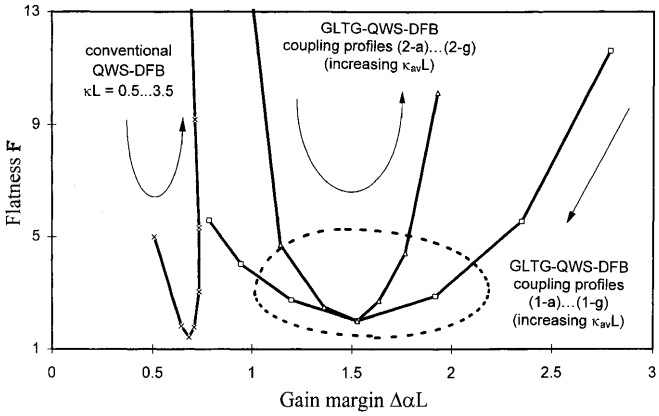

Fig. 2. Threshold chart (intra-cavity field flatness F versus gain margin $\Delta\alpha L$) of the GLTG-QWS-DFB lasers summarized in Table 1. Note that $\Delta\alpha L$ may be much higher than that of conventional QWS-DFBs, shown as a comparison (the κL step in this latter case is 0.5 with an extra point, the one provided with the lowest F, at $\kappa L = 1.25$). Good modal stability is expected in the region approximately bounded by the *dashed ellipse*

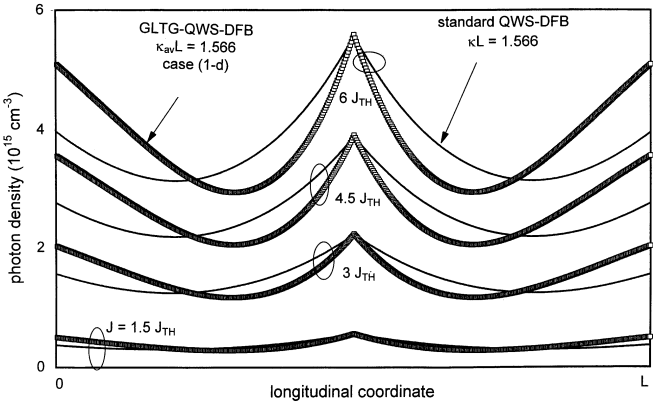

Fig. 3. Photon density longitudinal profile for several values of the bias current. The GLTG-QWS-DFB laser exhibits an enlargement of the photon density near the facets with respect to the standard QWS-DFB laser, leading to an larger output optical power

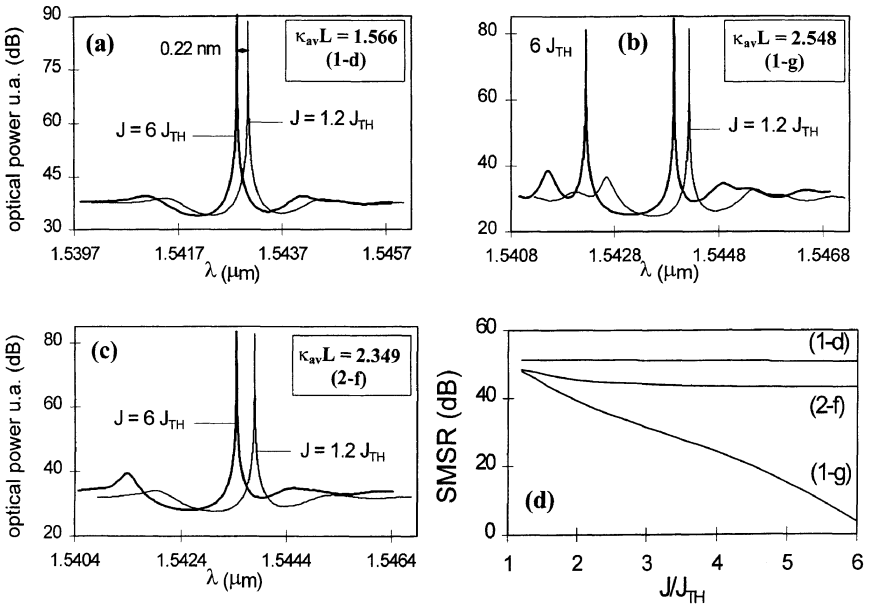

Fig. 4. (**a**–**c**) Emission spectra above threshold ($J = 1.2J_{TH}$ and $6J_{TH}$) of GLTG-QWS-DFBs (1-d), (1-g) and (2-f) as they appear in Table 1. **d**: Corresponding SMSR versus normalized current density

are liable to affect this wavelength shift, are not included in our calculations.

Higher κL products being desirable, structures (1-g) and (2-f) have been simulated (κL around 2.5). In the first case (Fig. 4b), the spectrum becomes rapidly bimodal due to the poor threshold performance (see Table 1). In fact, this particular coupling configuration is very close to the strongly coupled standard QWS-DFB which is known to be very senstive to SHB above threshold. The resulting SMSR tends towards zero. On the other hand, structure (2-f) is less sensitive to SHB because of its very high gain margin. A side mode grows up but remains negligible and the SMSR decreases very slightly. This shows that strongly coupled GLTG devices may remain single-mode provided that κ exhibits a gaussian shape which departs from the uniformly coupled QWS-DFB configuration.

4 Conclusion

QWS-DFB lasers with a coupling coefficient following a gaussian-like longitudinal profile have been theoretically studied. Such an approach can prove of interest in the design of DFB devices provided with very large gain margins and sufficiently flat intra-cavity fields, and consequently insensitive to spatial hole burning. These specific structures may also exhibit an enlarged output optical power with respect to conventional QWS-DFB lasers and could help to achieve single-mode high-power operation.

Acknowledgements. The author wishes to thank Dr Y. Boucher for helpful and stimulating discussions.

References

1. H. Soda, Y. Kotaki, H. Sudo, H. Ishikawa, S. Yamakoshi, H. Imai: IEEE J. Quantum Electron. **QE-23**, 804 (1987)
2. J.E. Whiteaway, G.H.B. Thompson, A.J. Collar, C.J. Armistead: IEEE J. Quantum Electron. **QE-25**, 1261 (1989)
3. B.S.K. Lo, H. Ghafouri-Shiraz: IEEE J. Lightwave Technol. **13**, 200 (1995)
4. T. Fessant, J. Le Bihan: Semiconductor and Integrated Optoelectronics Conference, SIOE'95, Cardiff (1995)
5. G. Morthier, K. David, P. Vankwikelberge, R.G. Baets: IEEE Photonics Technol. Lett. **2**, 388 (1990)
6. J.I. Kinoshita, K. Matsumoto: IEEE J. Quantum Electron. **QE-25**, 1324 (1989)
7. T. Kimura, A. Sugimura: IEEE J. Quantum Electron. **QE-25**, 678 (1989)
8. P. Zhou, G.S. Lee: Electron. Lett. **26**, 1660 (1990)
9. J. Salzman, H. Olesen, A. Moller-Larsen, O. Albrektsen, J. Hanberg, J. Norregaard, B. Jonsson, B. Tromborg: IEEE J. Select. Topics Quantum Electron. **1**, 346 (1995)
10. H. Hillmer, A. Grabmaier, S. Hansmann, H. Burkhard: Electron. Lett. **30**, 1483 (1994)
11. H. Soda, K. Wakao, H. Sudo, T. Tanahashi, H. Imai: Electron. Lett. **20**, 1016 (1984)
12. H. Soda, H. Ishikawa, H. Imai: Electron. Lett. **22**, 1047 (1986)
13. T. Fessant: Opt. Commun. **148**(1–3), 171 (1998)
14. V.N. Seminogov, A.I. Khudobenko, V.Y. Panchenko, V.I. Sokolov: SPIE Proc. **2382**, 224 (1995)
15. V.I. Sokolov, V.Y. Panchenko, V.N. Seminogov: SPIE Proc. **2682**, 176 (1996)
16. Y. Boucher, O. Dellea, J. Le Bihan: IEEE J. Quantum Electron. **QE-33**, 2137 (1997)